Competitive and cooperative anisotropy in magnetic nanocrystal chains of magnetotactic bacteria

D. Koulialias,[1,2] I. García-Rubio,[3,4] L. Rahn-Lee,[5,a)] A. Komeili,[5] J. F. Löffler,[2] A. U. Gehring,[1] and M. Charilaou[2,b)]
[1]*Institute of Geophysics, Department of Earth Sciences, ETH Zurich, 8092 Zurich, Switzerland*
[2]*Laboratory of Metal Physics and Technology, Department of Materials, ETH Zurich, 8093 Zurich, Switzerland*
[3]*Laboratory of Physical Chemistry, Department of Chemistry, ETH Zurich, 8093 Zurich, Switzerland*
[4]*Centro Universitario de la Defensa, 50090 Zaragoza, Spain*
[5]*Department of Plant and Microbial Biology, University of California, Berkeley, California 94720, USA*

(Received 3 May 2016; accepted 6 August 2016; published online 22 August 2016)

The formation of cellular magnetic dipoles by chain assemblies of stable single-domain magnetite nanocrystals is a characteristic feature in magnetotactic bacteria (MTB). The dipole strength depends on the competition or cooperation between the various anisotropic energy contributions, mainly between the magnetocrystalline and the interaction-induced shape anisotropy. Ferromagnetic resonance spectroscopy and numerical simulations of intracellular magnetite assemblies in the MTB *Desulfovibrio magneticus* strain RS-1 show that the alignment of elongated nanocrystallites leads to a predominant uniaxial anisotropy, which is enhanced when the magnetocrystalline symmetry is collinear to the chain, i.e., the anisotropies are cooperative *vs.* being competitive. This direct insight into the anisotropy variations in chain assemblies provides a physical framework to tailor magnetic nanocomposites, where the collective magnetic properties result from the interactions between the individual nanocrystalline constituents. *Published by AIP Publishing.*
[http://dx.doi.org/10.1063/1.4961321]

I. INTRODUCTION

Magnetic nanocrystallites organized in chain assemblies exhibit remarkable properties that do not exist if the nanocrystallites are dispersed or clumped together in bulk materials. This is because of the competition between particle-specific properties and those generated by their organization. Chain assemblies of nanocrystallites are therefore an ideal test ground to study the physics of many-body systems, with considerable scientific interest and technological applications in areas such as diagnostic biomedicine, cancer therapy, data storage, or ferrofluid-based devices.[1–8] In this context, magnetotactic bacteria (MTB) have gained special attention.[9–11] This heterogeneous group of bacteria biomineralizes in their cells magnetic nanocrystallites, generally magnetite (Fe_3O_4), encapsulated by lipid bilayers known as magnetosomes, that are organized in chains by a skeletal filament.[12–14] The mineral-chemical properties and shape of the nanocrystallites are genetically codified, and therefore strain-specific. The linear arrangement generates a strong magnetic dipole that is used as a compass to navigate MTB along the Earth's magnetic field lines towards favorable habitats.[15,16] The chain configuration and the resulting anisotropy properties are also a key to magnetically detect MTB in environmental systems[17–21] and thus infer the microbial evolution of the planet based on their magnetic properties.

The various groups of MTB differ in their strategy to reach optimal cellular dipole moments by forming different crystallite sizes and morphologies and/or by the arrangement with respect to their magnetic easy axis.[22] There exist MTB strains with genetic blueprints that enable the synthesis of nearly equidimensional magnetite biominerals with their [111] easy axes parallel to the long chain axis, which is generally the cell axis.[23,24] This configuration generates a strong interaction-induced shape anisotropy, i.e., a dipolar system with cooperative magnetocrystalline anisotropy of the crystallites and shape anisotropy of the chain assemblies.[25,26] There are also MTB, which form bullet-shaped magnetite nanocrystallites arranged along their [001] hard axes.[27–29] In this case, the magnetocrystalline and the shape anisotropies are non-parallel and form a competitive system (see Fig. 1(c)), which, nonetheless, also results in an intra-cellular magnetic dipole aligned with the long axis of the chain, specifically due to the elongation of the crystallites along the [100] axis.[30,31]

The separation and quantification of the different anisotropy contributions and their change during a shift from a competitive to a cooperative system and *vice versa* are of fundamental interest to understand magnetotaxis in living organisms and to build bio-inspired magnetic nanocomposites with tunable anisotropy properties. The ideal candidates to explore this shift are MTB with magnetite crystallites arranged along the [001] hard axes, because pure magnetite undergoes a low-temperature transition, known as Verwey transition with $T_v \approx 120\,\mathrm{K}$. In this case, the crystallographic structure changes from cubic to monoclinic and the magnetic easy axis switches from [111] to [001] upon cooling,[32,33] i.e., the anisotropy system transforms from competitive

a)Present address: William Jewell College, 500 College Hill, Liberty, Missouri 64068, USA.
b)Author to whom correspondence should be addressed. Electronic mail: michalis.chariloau@mat.ethz.ch.

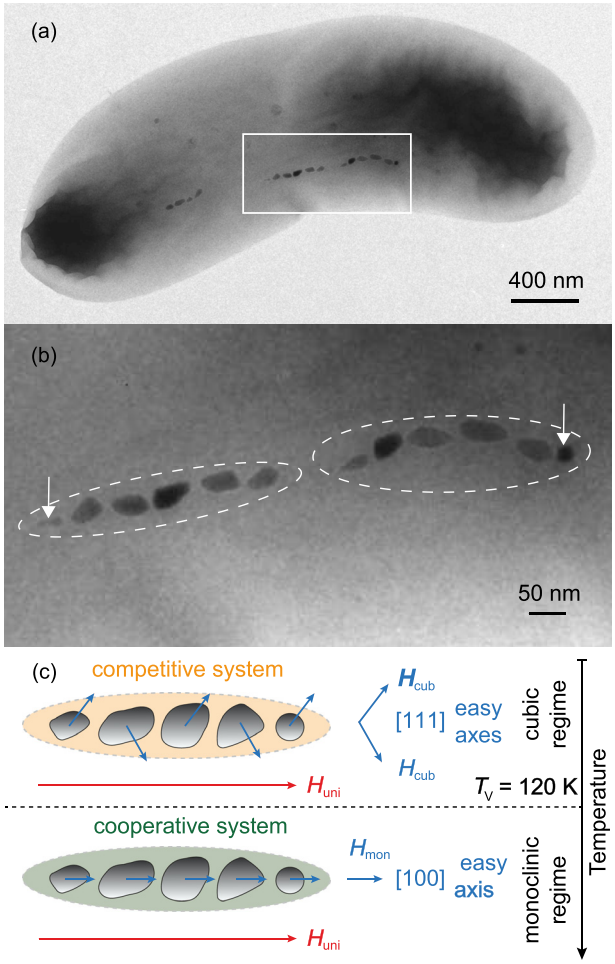

FIG. 1. (a) Transmission electron microscopy micrograph of a single MTB cell with magnetite nanocrystallites organized in chains. (b) A closer look of the stable single-domain nanocrystallites exhibits variable morphologies with a general arrangement along their [100] axes, as indicated; crystallites of less than 30 nm in size occur at the ends of the chains (arrowed) and were produced in an early crystallization step. (c) Schematic display of competitive and cooperative anisotropy configurations.

above T_v to cooperative below T_v. Among the MTB, *Desulfovibrio magneticus* strain RS-1 is the only strain with bullet-shaped nanocrystallites aligned along the [001] hard axis that has been cultured under laboratory conditions.[27,34,35] The typical crystallographic and magnetic properties of the nanocrystallites in cultured RS-1 cells are also well known. Here, we use this strain in a multi-frequency ferromagnetic resonance (FMR) spectroscopic analysis, which gives detailed insight into the critical effect of anisotropy configuration on the magnetic properties of chain assemblies. This provides a deeper understanding of how to tailor magnetic nanocomposites and nanomaterials to optimize their properties.

II. EXPERIMENTAL DETAILS

The cells of *D. magneticus* strain RS-1 were cultured in a medium, as previously reported,[36] except that 25 mM 4-(2-hydroxyethyl)-1-piper-azineethanesulfonic acid was added to the growth media and the pH was set to 6.7. The samples were collected at an early stationary phase. The nanostructure of the MTB was investigated using transmission electron microscopy (TEM), as described in Ref. 36.

For FMR measurements, a cell dispersion was lyophilized and subsequently fixed in paraffin inside an EPR (electron paramagnetic resonance) quartz tube for the X-band and in a glass capillary for the Q-band. The FMR spectra were recorded at X- and Q-band frequencies, i.e., at 9.8 GHz and 34.2 GHz, respectively, with Bruker E500/E560 spectrometers equipped with temperature controllers and helium gas-flow cryostats from Oxford Instruments. The experimental temperatures were set in the range between 50 K and 300 K. The experimental FMR spectra were fitted with calculated spectra, based on micromagnetic theory as outlined below, in order to extract the magnetic anisotropy in absolute units.

III. RESULTS AND DISCUSSION

A. Morphology and arrangement of the nanocrystallites

Cultures of the RS-1 strain were grown as previously reported[36] (see also Section II). Transmission electron micrographs (Figs. 1(a) and 1(b)) showed bacteria with several intracellular assemblies consisting of generally less than 10 nanocrystallites with spacing (d) of about 15 nm in one-dimensional arrangements developed along the center line of the cell. The distances between the chain assemblies vary and often exceed 100 nm. Magnetostatic interactions between the chains can be ignored, considering that the energy density of dipole-dipole interactions decreases with d^3, and, therefore, the inter-chain interactions have about 1000 times lower energy than the intra-chain interactions. With this in mind, the cellular magnetic dipole is the vector sum of the dipoles of individual chains. The magnetite nanocrystallites exhibit irregular bullet-shaped morphology characteristic of the strain RS-1.[27,34] As previously reported,[31] the average length of the nanocrystallites in our cultured RS-1 strain is 53.8 ± 14.2 nm, which is above the threshold for non-interacting stable single-domain (SSD) magnetite.[37,38] In addition to the SSD nanocrystallites, smaller spherical particles of about 20 nm in size occur at the ends of the chains [Figure 1(b)]. It has been shown for several MTB species including strain RS-1 that bullet-shaped magnetite crystallizes in a two-step process along different crystallographic axes, and, therefore, the nearly equidimensional small particles represent most likely the first crystallization step.[23,29,30,36] The major part of the nanocrystallites has grown along [100], which is the magnetic hard axis of magnetite.[27] Thus, the magnetic anisotropies in the RS-1 strain form a competitive system at room temperature (Fig. 1(c)).

B. Analytical description of anisotropy in magnetic chain assemblies

In our calculations, we treat each chain as a Stoner-Wohlfarth-type particle[39,40] and consider two anisotropy contributions (Fig. 1(c)): the uniaxial shape anisotropy field H_{uni} from the linear alignment, i.e., implicit inter-crystallite dipolar interactions, and uniaxial contributions of each particle, and the crystal anisotropy field H_{cryst} originating from

each crystallite.[41] The different contributions to the total energy density are therefore:

(i) the Zeeman energy term, i.e., the interaction with the external field

$$F_Z = -M H_{ext} [\sin\theta \sin\theta_H \cos(\varphi - \varphi_H) + \cos\theta \cos\theta_H], \quad (1)$$

where M is the magnetization, H_{ext} is the external field, and θ, θ_H and φ, φ_H are the polar and azimuthal angles of the magnetization and of the external magnetic field vector, respectively;

(ii) the shape (uniaxial) anisotropy energy term, i.e., the magnetostatic self-energy

$$F_{self} = 2\pi N_{eff} M^2 \sin^2\theta = \frac{1}{2} H_{uni} M \sin^2\theta, \quad (2)$$

where $N_{eff} = N_{\parallel} - N_{\perp}$ is the effective demagnetizing factor ($N_{\parallel}$ parallel to the chain and $N_{\perp}$ perpendicular to the long chain axis); and

(iii) the magnetocrystalline anisotropy energy F_{cryst}. Here, we consider two scenarios, i.e., above T_V, where the cubic [111] axis is the easy axis of magnetization, and below T_V, where the monoclinic [100] axis is the easy axis of magnetization. In the cubic structure, the energy density of the magnetocrystalline field is

$$F_{cryst}^{cub} = K_1 \sin^2\theta - \frac{K_1}{8} (\cos 4\varphi + 7) \sin^4\theta, \quad (3)$$

where $K_1 = M H_{cub}$ is the first-order anisotropy constant of magnetite ($K_1 = -1.1 \times 10^5$ ergs/cm^3 at 300 K). In the monoclinic phase, i.e., below T_V, the energy density of the crystalline anisotropy field, considering the symmetry of the monoclinic lattice as shown in Ref. 42, is

$$F_{cryst}^{mon} = \frac{1}{2} K_{u,eff} \sin^2\theta - \frac{K_{mon}}{2} (\sin^2\theta \cos^2\varphi - 2 \sin\theta \cos\theta \cos\varphi), \quad (4)$$

where $K_{mon} = M H_{mon}$ is a monoclinic term that takes into account a canting effect of the easy axis from the [100] towards the [111] direction and $K_{u,eff} = K_a + K_b + K_{mon}$ is the effective magnetocrystalline uniaxial field, with the angles θ and φ measured as before (K_a and K_b are crystal fields along the a- and b-axes of the monoclinic structure). Because the effective magnetocrystalline uniaxial term has the same angle dependence as the shape uniaxial field from Eq. (2), it is incorporated in the total uniaxial field H_{uni}. The total energy density for a single chain is then $F = F_Z + F_{self} + F_{cryst}$.

The experimental determination of the different anisotropy contributions in intracellular magnetite chains is performed by Ferromagnetic Resonance (FMR) spectroscopy.[43,44] In an FMR experiment, the magnetization performs a precessional motion (Larmor precession) upon the application of a sweeping dc magnetic field. At the same time, a microwave magnetic field with a constant frequency is transversely superimposed and resonance occurs when the Larmor frequency matches the microwave frequency, i.e., when maximum absorption of microwave energy takes place. This is described by the resonance equation $\omega = \gamma \cdot H_{res}$, where ω is the microwave frequency, $\gamma = \frac{2\pi g \mu_B}{h}$ is the gyromagnetic ratio, and H_{res} is the resonance magnetic field, which includes the external magnetic field H_{ext} and the internal anisotropy fields H_{int}, i.e., at resonance $H_{res} = H_{eff} = H_{ext} + H_{int}$.

For the simulation of the experimental FMR spectra from the above expression of the total energy density, we calculate the resonance field H_{res} from the resonance equation[45]

$$H_{res}^2 = \left(\frac{\omega}{\gamma}\right)^2 = \frac{1}{M^2}\left[\partial_{\theta\theta}F\left(\frac{\partial_{\varphi\varphi}F}{sin^2\theta} + \frac{\cos\theta}{\sin\theta}\partial_\theta F\right) - \left(\frac{\partial_{\theta\varphi}F}{\sin\theta} - \frac{\cos\theta}{sin^2\theta}\partial_\varphi F\right)^2\right], \quad (5)$$

where $\partial_\theta F$, $\partial_{\theta\theta}F$, $\partial_\varphi F$, and $\partial_{\varphi\varphi}F$ are the first and second-order derivatives of the energy density with respect to θ and φ, respectively. The resonance equation is solved at equilibrium, i.e., at $\partial_\theta F = 0$ and $\partial_\varphi F = 0$, and the values of the resonance field are obtained at each set of field angles θ_H and ϕ_H. A uniform distribution of the crystallite orientations is assumed for the calculations. Each resonance event is described by the Landau-Lifshitz-Gilbert equation of motion

$$\partial_t \vec{M} = -\gamma (\vec{M} \times \vec{H}_{eff}) + \frac{G}{\gamma M^2} (\vec{M} \times \partial_t \vec{M}), \quad (6)$$

with $\partial_t \vec{M}$ being the time derivative of the magnetization and G is the Gilbert damping frequency, where the solution is typically a Lorentzian or a Gaussian.

We then generate the FMR spectrum of an ensemble of randomly oriented chains by convoluting all the individual spectra. Hence, with this method, we use the two anisotropy fields, H_{uni} and H_{cryst}, and a convolution linewidth as inputs, fit the experimental data with the simulated FMR spectrum, and iterate the simulation to obtain the best fit of the experimental data. The Landé g-factor was set to the intrinsic value of magnetite ($g = 2.06$).

Considering the RS-1 strain, the intracellular chains, consisting of less than ten magnetite crystallites generally organized along the [100] hard axis, can in their entirety be modeled by prolate ellipsoids.[30,41] An average length-to-width aspect ratio of 1.8 ± 0.4, previously determined for our cultured RS-1 strain,[31] is equivalent to an effective demagnetizing factor of $N_{eff} = 0.215 \pm 0.085$. This corresponds to a uniaxial shape anisotropy field of 1.235 ± 0.460 kOe, based on Eq. (2). Thus, the uniaxial anisotropy field of each crystallite dominates over the cubic magnetocrystalline field, even above T_v, as will be discussed below.

C. Multi-frequency FMR spectra

For the experimental analysis of the anisotropy, FMR spectroscopy in the X-band at 9.8 GHz is complemented by

the Q-band mode at 34.2 GHz (see Section II). Considering the resonance equation $\omega = \gamma H_{res}$, the external field at which resonance occurs is lower in the X-band as compared to the Q-band by a factor proportional to the frequency ω. Figure 2 shows the characteristic FMR spectra of the RS-1 bulk sample taken at three different temperatures for (a) X- and (b) Q-band frequencies. In order to check the uniformity of the spatial distribution of the bacteria in the bulk sample, the FMR spectra were recorded at different orientations, and the absence of an angular dependence indicates a highly uniform distribution of the magnetic chains. At room temperature, the X-band spectrum exhibits two main features at about 2.5 kOe and 4.5 kOe, which are caused by the superposition of resonances from the randomly distributed chains. The low-field feature is due to contributions from the easy magnetization of chains nearly parallel to the long cell axes, whereas the high-field feature arises from the hard magnetization perpendicular to these cell axes.[31,46] At the Q-band, the spectral shape at correspondingly higher fields is the same as at the X-band. Here, the low- and high-field features are around 11 kOe and 13 kOe, respectively. The difference between the features, as a measure of the total magnetic anisotropy, is about 2 kOe for both the X- and Q-band spectra.

At 160 K, the overall spectra show little changes and the total magnetic anisotropy increases slightly. When, however, we cool down to temperatures below T_V, e.g., to 90 K, the X-band spectrum changes dramatically as opposed to the Q-band, which only shows little changes. At the X-band, the linewidth increases strongly and the low-field peak is shifted to much lower field strengths ($\sim$0.7 kOe at 90 K).

The abrupt change in the spectral response below 120 K is due to the Verwey transition with a corresponding crystallographic change from cubic to monoclinic and the consequent shift of the easy-axis magnetization from [111] to [100]. This shift triggers the conversion of the system from competitive to cooperative anisotropy. We quantify this conversion by fitting the experimental FMR spectra with the model discussed above and extract the crystalline and uniaxial anisotropy fields. As seen in Fig. 2, the most important features, i.e., peak position and intensity, of the experimental and calculated spectra are in very good agreement, enabling us to extract the anisotropy with good precision. The uniaxial field determines the distance between the low-field and high-field features, whereas the crystal field determines the fine structure of the spectrum and the relative peak intensities. Note that with decreasing temperature, the peak linewidth increases because of an enhanced overall anisotropy.

The temperature dependence of these two anisotropy fields is shown in Fig. 3. At room temperature, we obtain a crystalline anisotropy field of $H_{cryst} = -130 \pm 5$ Oe. With decreasing temperature, the crystal field slightly decreases to a minimum at about 240 K. Upon further cooling, H_{cryst} increases and changes sign at the isotropic point of 135 K. Below T_V, in the monoclinic regime, the crystal field exhibits a strong decrease upon cooling and reaches a value of -500 ± 10 Oe at low temperature (Fig. 3(a)). The values for H_{cryst} at X- and Q-bands are in good agreement, with the exception at $T = 160$ K (to be discussed below). The temperature dependence of the crystal field is very close to that of Fe_3O_4 single crystals[42,47] and the isotropic point agrees well with the value of 130 K for stoichiometric Fe_3O_4.[47] A similar behavior was found for the MTB *Magnetospirillum gryphiswaldense*, forming a system with cooperative anisotropies at $T > T_V$.[48,49] We note, however, that the absolute values of the crystal field at room temperature are significantly lower than the value of $H_{cryst} = -250$ Oe for magnetite in single

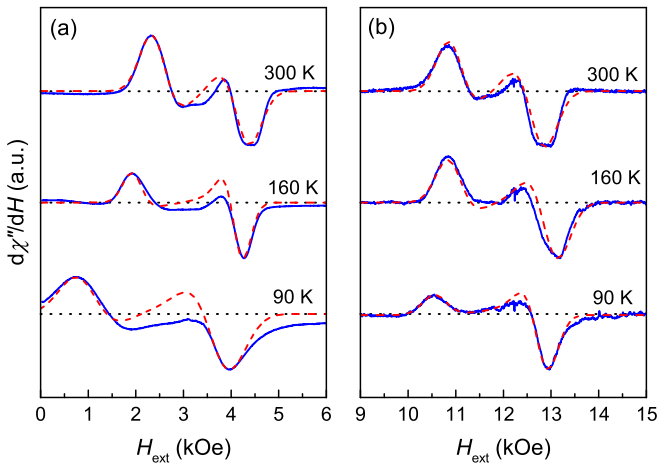

FIG. 2. Ferromagnetic resonance spectra, i.e., first derivative of the high-frequency susceptibility tensor *vs.* external DC field of MTB at (a) X-band and (b) Q-band, at $T = 300$ K, 160 K, and 90 K, respectively. Solid lines correspond to experiments and dashed lines correspond to theoretical calculations. Horizontal dotted lines indicate the baseline for each resonance.

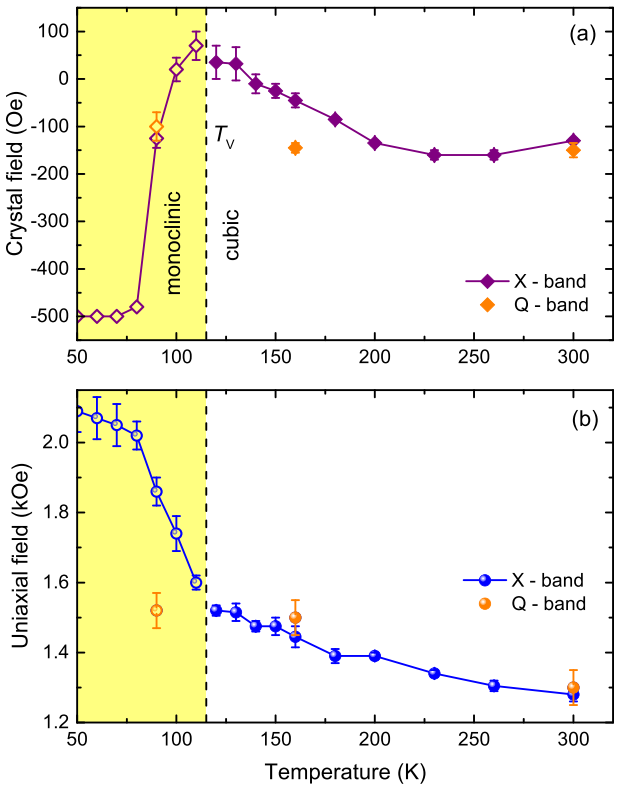

FIG. 3. Temperature dependence of the anisotropy fields showing (a) the crystalline field and (b) the uniaxial anisotropy field. The vertical dashed lines indicate the Verwey transition ($T_V = 120$ K), separating the cubic ($T > T_V$) from the monoclinic ($T < T_V$) regime.

crystals or in chains of *M. gryphiswaldense*.[41] The lower value for the RS-1 strain is probably an effect of the two-step crystal growth of bullet-shaped nanocrystallites along different crystal axes that leads to a competition of anisotropy easy axes even within single magnetosomes. Such effect is not accounted for in our calculations.

The changes of the crystal field as a function of temperature strongly affect the uniaxial anisotropy field. At room temperature, $H_{uni} = 1.28 \pm 0.02$ kOe, which is an order of magnitude larger than H_{cryst}. This shows that uniaxiality dominates the crystal field due to the organization of elongated, individual nanocrystallites in a chain assembly.

With decreasing temperature, H_{uni} increases monotonically, and below T_V it exhibits a prominent increase in the X-band mode. Below T_V, [100] becomes the easy axis of the magnetization, i.e., the magnetocrystalline anisotropy field is now parallel to the uniaxial field and we have a cooperative system (Fig. 1(c)). The alignment of the two anisotropy fields results in a strong uniaxial field, which at $T = 50$ K reaches 2.09 ± 0.06 kOe. This field is clearly larger than the uniaxial field of a single elongated magnetosome, where $H_{uni} \sim 1.2$ kOe.

Importantly, the values we obtain for H_{uni} at the X- and Q-bands are identical for $T > T_V$ but differ strongly for $T < T_V$. At 90 K, the value of the uniaxial anisotropy field at the X-band is 1.86 ± 0.04 kOe, whereas at the Q-band it is only 1.52 ± 0.05 kOe. To explain this difference, we have to consider the magnetization state of the sample at the resonance field H_{res}. In the Q-band mode, the resonance condition is fulfilled at high external fields, and the magnetization of the sample is fully saturated. In contrast, at the X-band, the resonance condition is fulfilled at an external field where the sample is not saturated, and the resonance is critically affected by the strength of the internal field. This is an important aspect to consider as our calculations assume saturated magnetization. In a non-saturated state, the equilibrium and resonance conditions differ strongly and this is the reason for the deviation in H_{uni} between the X- and Q-bands. To reconcile this, we consider the resonance condition for a purely uniaxial system along the easy axis, which is simply $H_{eff} = H_{iso} - H_{uni}$,[41] where H_{iso} is the resonance field for an isotropic system, and the fact that the crystalline uniaxial field is proportional to K_1/M. When M is smaller than the saturation value M_s, the anisotropy field H_{uni} increases which in turn decreases the resonance field along the easy axis. Hence, at the X-band, the low-field peak of the FMR spectrum, which corresponds to the resonances along the easy axes, occurs at a lower field because $K < M_s$. This scenario is similar to that previously reported[46,50] where X-band and S-band (4.2 GHz) spectra are compared and the remanence plays an important role for the latter. Moreover, the impact of the non-saturated state on the interpretation of the anisotropy contributions is much stronger on the uniaxial field than on the magnetocrystalline field. This is due to the fact that H_{uni} is determined by the distance between the low-field and high-field peaks, whereas H_{cryst} is determined close to the isotropic point, i.e., at a field where the sample is mostly saturated.

At this point, we compare our results with X-band FMR data obtained from *M. gryphiswaldense* strain MSR-1, which produces numerous, nearly equidimensional nanocrystallites organized in perfect chains and where the anisotropy fields are parallel at $T > T_V$.[26,49] This configuration generates a uniaxiality that can be considered as nearly pure interaction-induced shape anisotropy. At room temperature, *M. gryphiswaldense* strain MSR-1 exhibits a H_{uni} of about 1 kOe that is slightly lower than for the RS-1 strain.[41] For *M. gryphiswaldense*, the change in the anisotropy contribution across T_V occurs in the opposite way, i.e., the system is cooperative at high temperature but competitive at lower temperatures. This leads to the vanishing of a pronounced uniaxiality upon crossing T_V, as documented by broad FMR spectra without two characteristic resonance features.[49] Comparing the two strains RS-1 and MSR-1, the uniaxiality of one-dimensional, magnetic nanocomposites may be optimized by building blocks with pronounced shape anisotropy (e.g., bullet-shaped particles or nanorods) rather than by increasing the length of the chains.

IV. CONCLUSION

The FMR spectral analysis of the RS-1 strain exhibits a competitive interplay of anisotropies because of the organization of intracellular magnetite nanocrystallites predominantly along their [100] hard axis and due to the pronounced uniaxiality of the shape with a linear alignment of the nanocrystallites above T_V. The structural change at T_V, where the [100] direction becomes the easy axis of magnetization, triggers the change to a cooperative system, which is reflected in the X-band mode by a drastic increase in the uniaxial field. This FMR manifestation of the uniaxiality below the Verwey transition is because the magnetic nanocrystals are not fully saturated in the entire absorption range of the X-band, whereas the Q-band mode covers a magnetic field range where magnetite is fully saturated. The results obtained from the multi-frequency FMR analysis demonstrate how the balance between different sources of magnetic anisotropy in nanostructures is affected by the competition between anisotropy fields. This finding is crucial for the development of magnetic nanocomposites with specifically tailored anisotropy properties and may also help to detect MTB and their magnetic remains in geological environments.

ACKNOWLEDGMENTS

This project was supported by the Swiss National Science Foundation (Grant No. 200021-153173).

[1]Q. A. Pankhurst, J. Connolly, S. K. Jones, and J. Dobson, J. Phys. D: Appl. Phys. **36**, R167 (2003).
[2]S. Martel, C. C. Tremblay, S. Ngakeng, and G. Langlois, Appl. Phys. Lett. **89**, 233904 (2006).
[3]E. Alphandéry, Y. Ding, A. T. Ngo, Z. L. Wang, L. F. Wu, and M. P. Pileni, ACS Nano **3**, 1539 (2009).
[4]Y. Zhang, L. Sun, Y. Fu, Z. C. Huang, X. J. Bai, Y. Zhai, J. Du, and H. R. Zhai, J. Phys. Chem. C **113**(19), 8152 (2009).
[5]C. Martinez-Boubeta, K. Simeonidis, A. Makridis, M. Angelakeris, O. Iglesias, P. Guardia, A. Cabot, L. Yedra, S. Estrade, F. Peiro, Z. Saghi, P. A. Midgley, I. Conde-Leborán, D. Serantes, and D. Baldomir, Sci. Rep. **3**, 1652 (2013).

[6]G. Singh, H. Chan, A. Baskin, E. Gelman, N. Repnin, P. Král, and R. Klajn, Science **345**, 1149 (2014).
[7]S. Mannucci, L. Ghin, G. Conti, S. Tambalo, A. Lascialfari, T. Orlando, D. Benati, P. Bernardi, N. Betterle, R. Bassi, P. Marzola, and A. Sbarbati, PLoS One **9**, e108959 (2014).
[8]J. F. Löffler, H. B. Braun, and W. Wagner, Phys. Rev. Lett. **85**, 1990 (2000).
[9]I. A. Banerjee, L. Yu, M. Shima, T. Yoshino, H. Takeyama, T. Matsunaga, and H. Matsui, Adv. Mater. **17**, 1128 (2005).
[10]T. Prozorov, D. A. Bazylinski, S. K. Mallapragada, and R. Prozorov, Mater. Sci. Eng., R **74**, 133 (2013).
[11]I. Kolinko, A. Lohße, S. Borg, O. Raschdorf, C. Jogler, Q. Tu, M. Pósfai, E., Tompa, J. M. Plitzko, A. Brachmann, G. Wanner, Müller, Y. Zhang, and D. Schüler, Nat. Nanotechnol. **9**, 193 (2014).
[12]A. Scheffel, M. Gruska, D. Faivre, A. Linaroudis, J. M. Plitzko, and D. Schüler, Nature **440**, 110 (2006).
[13]A. Komeili, Z. Li, D. K. Newman, and G. J. Jensen, Science **311**, 242 (2006).
[14]C. T. Lefèvre and D. A. Bazylinski, Microbiol. Mol. Biol. Rev. **77**, 497–526 (2013).
[15]R. Blakemore, Science **190**, 377 (1975).
[16]D. A. Bazylinksi and R. B. Frankel, Nat. Rev. Microbiol. **2**, 217 (2004).
[17]B. P. Weiss, S. S. Kim, J. L. Kirschvink, R. E. Kopp, M. Sankaran, A. Kobayashi, and A. Komeili, Earth Planet. Sci. Lett. **224**, 73 (2004).
[18]R. E. Kopp, C. Z. Nash, A. Kobayashi, B. P. Weiss, D. A. Bazylinski, and J. L. Kirschvink, J. Geophys. Res. **111**, B12S25, doi:10.1029/2006JB004529 (2006).
[19]J. Li, W. Wu, Q. Liu, and Y. Pan, Geochem., Geophys., Geosyst. **13**, Q10Z51, doi:10.1029/2012GC004384 (2012).
[20]A. U. Gehring, J. Kind, M. Charilaou, and I. García-Rubio, Earth Planet. Sci. Lett. **309**, 113 (2011).
[21]L. Chang, A. P. Roberts, M. Winklhofer, D. Heslop, M. J. Dekkers, W. Krijgsman, J. D. Fitz Gerald, and P. Smith, J. Geophys. Res. **119**, 6136, doi:10.1002/2014JB011213 (2014).
[22]M. Pósfai, C. T. Lefèvre, D. Trubitsyn, D. A. Bazylinski, and R. B. Frankel, Front. Microbiol. **4**, 344 (2013).
[23]S. Mann, N. H. C. Sparks, and R. P. Blakemore, Proc. R. Soc. London, Ser. B **231**, 477 (1987).
[24]B. Devouard, M. Pósfai, X. Hua, D. A. Bazylinski, R. B. Frankel, and P. R. Buseck, Am. Mineral. **83**, 1387 (1998).
[25]D. Faivre, A. Fischer, I. García-Rubio, G. Mastrogiacomo, and A. U. Gehring, Biophys. J. **99**, 1268 (2010).
[26]M. Charilaou, J. Kind, I. García-Rubio, D. Schüler, and A. U. Gehring, Appl. Phys. Lett. **104**, 112406 (2014).
[27]M. Pósfai, B. M. Moskowitz, B. Arató, D. Schüler, C. Flies, D. A. Bazylinski, and R. B. Frankel, Earth Planet. Sci. Lett. **249**, 444 (2006).
[28]C. T. Lefèvre, M. Pósfai, F. Abreu, U. Lins, R. B. Frankel, and D. A. Bazylinski, Earth Planet. Sci. Lett. **312**, 194 (2011).
[29]J. Li, N. Menguy, C. Gatel, V. Boureau, E. Snoeck, G. Patriarche, E. Leroy, and Y. Pan, J. R. Soc., Interface **12**, 20141288 (2015).
[30]A. Körnig, M. Winklhofer, J. Baumgartner, T. Perez Gonzalez, P. Fratzl, and D. Faivre, Adv. Funct. Mater. **24**, 3926 (2014).
[31]M. Charilaou, L. Rahn-Lee, J. Kind, I. García-Rubio, A. Komeili, and A. U. Gehring, Biophys. J. **108**, 1268 (2015).
[32]D. J. Dunlop and Ö. Özdemir, *Rock Magnetism*, Cambridge Studies in Magnetism (Cambridge University Press, 1997).
[33]F. Walz, J. Phys.: Condens. Matter **14**, R285 (2002).
[34]T. Sakaguchi, J. G. Burgess, and T. Matsunga, Nature **365**, 47 (1993).
[35]L. Rahn-Lee, M. E. Byrne, M. Zhang, D. Le Sage, D. R. Glenn, T. Milbourne, R. L. Walsworth, H. Vali, and A. Komeili, PLoS Genet. **11**(1), e1004811 (2015).
[36]M. E. Byrne, D. A. Ball, J.-L. Guerquin-Kern, I. Rouiller, T.-D. Wu, K. H. Downing, H. Vali, and A. Komeili, Proc. Natl. Acad. Sci. U. S. A. **107**, 12263 (2010).
[37]R. F. Butler and S. K. Banerjee, J. Geophys. Res. **80**, 4049, doi:10.1029/JB080i029p04049 (1975).
[38]A. R. Muxworthy and W. Williams, J. R. Soc., Interface **6**, 1207 (2009).
[39]E. C. Stoner and E. P. Wohlfarth, Philos. Trans. R. Soc., A **240**, 599 (1948).
[40]J. F. Löffler, H. B. Braun, W. Wagner, G. Kostorz, and A. Wiedenmann, Phys. Rev. B **71**, 134410 (2005).
[41]M. Charilaou, M. Winklhofer, and A. U. Gehring, J. Appl. Phys. **109**, 093903 (2011).
[42]K. Abe, Y. Miyamoto, and S. Chikazumi, J. Phys. Soc. Jpn. **41**, 1894 (1976).
[43]C. Kittel, Phys. Rev. **73**, 155 (1948).
[44]S. V. Vonsovskii, *Ferromagnetic Resonance* (Pergamon, Oxford, 1966).
[45]L. Baselgia, M. Warden, F. Walder, S. L. Hutton, J. E. Drumheller, Y. Q. He, P. E. Wigen, and M. Maryško, Phys. Rev. B **38**, 2237 (1988).
[46]G. Mastrogiacomo, H. Fischer, I. García-Rubio, and A. U. Gehring, J. Magn. Magn. Mater. **322**, 661 (2010).
[47]L. R. Bickford, Phys. Rev. **78**, 449 (1950).
[48]H. Fischer, G. Mastrogiacomo, J. F. Löffler, R. J. Warthmann, P. G. Weidler, and A. U. Gehring, Earth Planet. Sci. Lett. **270**, 200 (2008).
[49]A. U. Gehring, H. Fischer, M. Charilaou, and I. García-Rubio, Geophys. J. Int. **187**, 1215 (2011).
[50]A. U. Gehring, J. Kind, M. Charilaou, and I. García-Rubio, J. R. Soc., Interface **10**, 20120790 (2012).